Porous Poly(ε-Caprolactone) Scaffolds for Retinal Pigment Epithelium Transplantation

Kevin J. McHugh,[1–3] Sarah L. Tao,[*,3] and Magali Saint-Geniez[1,4]

[1]Schepens Eye Research Institute, Boston, Massachusetts
[2]Boston University, Boston, Massachusetts
[3]The Charles Stark Draper Laboratory, Inc., Cambridge, Massachusetts
[4]Harvard Medical School, Boston, Massachusetts

Correspondence: Magali Saint-Geniez, Schepens Eye Research Institute, 20 Staniford Street, Boston, MA 02114; magali_saintgeniez@meei.harvard.edu.

Current affiliation: *CooperVision, Inc., Pleasanton, California

Submitted: July 15, 2013
Accepted: January 25, 2014

Citation: McHugh KJ, Tao SL, Saint-Geniez M. Porous poly(ε-caprolactone) scaffolds for retinal pigment epithelium transplantation. *Invest Ophthalmol Vis Sci*. 2014;55:1754–1762. DOI:10.1167/iovs.13-12833

Purpose. Retinal pigment epithelium (RPE) transplantation is a promising strategy for the treatment of dry age-related macular degeneration (AMD). However, previous attempts at subretinal RPE cell transplantation have experienced limited success due to poor adhesion, organization, and function on aged or diseased Bruch's membrane. Instead, cell-based strategies may benefit from a synthetic scaffold that mimics the functions of healthy Bruch's membrane to promote the formation of a functional RPE monolayer while maintaining metabolite exchange between the vasculature and outer retina.

Methods. This study evaluated the behavior of human RPE on nanopatterned porous poly(ε-caprolactone) (PCL) film as a potential scaffold for therapeutic transplantation. Fetal human RPE (fhRPE) was cultured on porous PCL, nonporous PCL, or Costar porous polyester transwells for up to 8 weeks and assessed using light microscopy, fluorescent microscopy, transepithelial resistance, quantitative PCR, ELISAs, and phagocytosis assays.

Results. fhRPE on porous PCL displayed improved markers of maturity and function compared with both porous polyester transwells and nonporous PCL, including pigmentation, increased cell density, superior barrier function, up-regulation of RPE-specific genes, and polarized growth factor secretion.

Conclusions. This study indicates that porous PCL is an attractive scaffold for RPE transplantation. In addition to being biocompatible with the subretinal space, porous PCL also allows for trans-scaffold metabolite transport and significantly improves RPE cell behavior compared to nonporous PCL or porous polyester transwells.

Keywords: retinal pigment epithelium, age-related macular degeneration, in vitro, scaffold, porous polycaprolactone

Age-related macular degeneration (AMD) is the leading cause of blindness among the elderly.[1] AMD is a multifactorial, progressive disease of the central retina that can be divided into two distinct categories, wet (choroidal neovascularization) and dry (geographic atrophy). One of the first pathological hallmarks of dry AMD is the loss of functional retinal pigment epithelium (RPE), which normally supports the survival and function of both photoreceptors and vasculature.[2,3] However in AMD, RPE anomalies lead to irregular behavior and atrophy that contribute to downstream photoreceptor degeneration. As a result, therapeutic RPE transplantation represents an attractive strategy for halting the progression of retinal degeneration by restoring normal RPE function prior to permanent vision loss.[4] Unfortunately, past attempts to transplant RPE have failed because allografted cells were introduced without addressing other pathological changes to the host microenvironment such as Bruch's membrane (BrM) thickening, cross-linking, and drusen accumulation.[5–9]

Interestingly, some of the structural alterations to BrM have even been detected in dry AMD prior to RPE atrophy, suggesting that extracellular matrix changes occur soon after disease onset and likely contribute to downstream degeneration.[9,10] In vitro and in vivo studies have provided further evidence for the impact of age- and disease-related changes to BrM on RPE function. Healthy RPE seeded onto aged or diseased BrM in vitro show a dramatic decline in cell behavior, gene expression, and function.[11–15] In vivo experiments that injected RPE in suspension have yielded similarly poor results with minimal cell attachment, survival, and organization on the animal's native BrM.[15–17]

Therefore, effective cell-based strategies will likely require the co-implantation of a BrM substitute and mature, well-organized RPE to enhance cell survival and function.[18,19] Although extracellular matrix components could be assembled to form this type of support, synthetic polymers may be more attractive due to reproducibility, ease of modification, and nonimmunogenicity.[20–23]

Poly(lactic acid) (PLA) and poly(lactic-co-glycolic acid) (PLGA) were two of the first materials proposed for supporting RPE delivery[18,24]; however, despite their classification as generally biocompatible,[25] both materials have been shown to cause widespread retinal degeneration when implanted into the subretinal space.[19,26] This lack of tissue-specific biocompatibility is likely due to rapid degradation of these polymers (typically 1–18 months[27]), which leads to a buildup of acidic degradation products in the small subretinal space.[28] These products lower the microenvironmental pH leading to a major inflammatory response and associated retinal cell death. As a result, recent subretinal implant studies have focused on nondegradable or more slowly degrading polymers including poly(methyl methacrylate),[19,29] parylene, poly(ethylene glycol),[30] poly(ε-caprolactone) (PCL),[31] and poly(glycerol sebacate).[32]

This study aimed to develop an RPE scaffold constructed from PCL, a material that has demonstrated high compatibility with the subretinal space of mice and pigs.[26,31] Although PCL, like PLA and PLGA, degrades via hydrolytic cleavage of ester bonds,[33] this occurs more slowly (typically over longer than 3 years[22,34]) and produces degradation products that are comparatively less acidic.[27] These differences help to minimize local alterations in pH and any associated inflammatory response.[25] A microfabrication-based approach was used to pattern PCL films with pores that support metabolite transport. This method resulted in PCL scaffolds with full-thickness pores that were small (<1 μm), well controlled, and highly reproducible—characteristics that have been identified as beneficial for ocular tissue engineering scaffolds.[16,35] These porous PCL scaffolds were tested in vitro to determine the effect of cell culture substrate properties on RPE maturation, gene expression, and function.

Methods

Scaffold Fabrication and Characterization

Scaffolds were created using the pore casting process our group has previously described.[36] Briefly, photolithography and deep reactive ion etching were used to produce a silicon mold with sub-micron cylindrical features protruding from its top surface. The mold was then covered with a PCL solution and spun at high speed resulting in a solid PCL film. The film was then peeled from the mold to yield a thin scaffold with full-thickness cylindrical pores.

Scaffold morphology including pore size and total porosity was determined using scanning electron microscopy (SEM). Prior to imaging, scaffolds were coated with approximately 20 nm of gold/palladium using a Cressington 108 sputter coater (Cressington Scientific Instruments, Watford, UK) for 25 seconds at 20 mA with a distance of 3 cm. Images were then collected using a Zeiss Supra 55VP Field Emission SEM (Carl Zeiss, Oberkochen, Germany) at 5.0 kV and subsequently analyzed in Adobe Photoshop (Adobe Systems, San Jose, CA). Porous PCL scaffold thickness was determined using an Alpha Step 500 Profiler (KLA-Tencor, Milpitas, CA) and qualitatively confirmed by comparing the visible height of the silicon cylinders with and without an adherent PCL film.

Cell Culture

Fetal human RPE cells (fhRPE) were purchased from Lonza Biologics (cat. no. 00194987; Allendale, NJ), expanded, and plated at passage 5 at high density (3×10^5 cells/cm^2) on porous PCL (700-nm pores), nonporous PCL, and Costar polyester transwells (400-nm track-etched pores; Corning, NY). Nonporous PCL and polyester transwells were used as controls for material and porosity, respectively. PCL samples were mounted on transwell supports devoid of their original membrane. All substrates were coated with 300 μL of 10 μg/mL laminin from Engelbreth-Holm-Swarm murine sarcoma basement membrane (cat. no. L2020; Sigma-Aldrich, St. Louis, MO) in PBS for 2 hours prior to cell culture. An ELISA confirmed that statistically similar amounts of laminin adsorbed to the surface of all substrates (data not shown), suggesting that changes in cell behavior are a direct result of culture substrate rather than an indirect function of laminin adsorption. After seeding, cells were maintained at 37°C, 5% CO_2 in serum-free, growth factor-free RtEBM media (Lonza, cat. no. 0019540) supplemented with 1% (v/v) GlutaMAX (Invitrogen, Carlsbad, CA) and 1% (v/v) penicillin-streptomycin (Lonza). Media were changed twice per week for up to 8 weeks.

Immunohistochemistry

All antibodies and reagents used in this study were purchased from Invitrogen and Sigma-Aldrich, respectively, unless otherwise noted. Cells were fixed for 10 minutes in 4% paraformaldehyde and permeabilized with 0.1% Triton X-100 in PBS for 5 minutes. After washing, samples were incubated for 2 hours in a blocking buffer containing of 3% (v/v) goat serum and 2.5% (w/v) bovine serum albumin in PBS. Samples were incubated overnight at 4°C in blocking buffer also containing 2.5 μg/mL rabbit-raised antibody for zona occludin 1 (ZO-1), a tight junction-associated protein. The following day samples were incubated in blocking buffer containing 6.7 μg/mL AlexaFluor 488 goat anti-rabbit and 10 μL/mL 4′,6-diamidino-2-phenylindole (DAPI) for 1 hour and then imaged using an Axioskop MOT 2 (Carl Zeiss Meditec, Dublin, CA). Cell size was evaluated by manually tracing cell borders defined by ZO-1 staining in Adobe Photoshop.

Transepithelial Resistance

Transepithelial electrical resistance (TER) was used to quantitatively assess fhRPE tight junction formation and scaffold coverage. TER was measured using an EVOM2 Voltohmmeter (World Precision Instruments, Inc., Sarasota, FL) as previously described.[36] Nonporous PCL film was not tested because the resistance of the substrate alone exceeded the reliable range of the instrument.

Gene Expression

fhRPE RNA was isolated using RNA-bee solution (IsoText Diagnostics, Friendswood, TX) according to the manufacturer's protocol. One microgram of RNA was reverse-transcribed using Superscript III (Invitrogen). Real-time PCR was performed using FastStart SYBR Green Master mix with the LightCycler 480 Real-Time PCR System (Roche Applied Science, Indianapolis, IN). The primer sequences used are listed in Table 1. Relative gene expression was determined using the delta-delta Ct method after normalizing sample loading with the housekeeping genes *GAPDH* and *HPRT1*.

Protein Secretion

Cell culture media conditioned for 72 hours was collected from the apical and basal chambers at 1 or 4 weeks and stored at –80°C until further use. Concentration of secreted vascular endothelial growth factor (VEGF) and pigment epithelium derived factor (PEDF) were measured using human ELISAs kits (R&D Systems, Minneapolis, MN, and BioProducts MD, Middletown, MD). A custom 19-analyte multiplex ELISA (Milliplex Map; EMD Millipore, Billerica, MA) for human cytokines and chemokines was used to measure fhRPE secretion of soluble epidermal growth factor (EGF), eotaxin, fibroblast growth factor (FGF)-2, CX3CL1 (fractalkine), granulocyte colony-stimulating factor (G-CSF), granulocyte-macrophage colony-stimulating factor (GM-CSF), CXCL1 (GRO), interleukin (IL)-1α, IL-1β, IL-1RA, IL-6, IL-8, IL-15, interferon γ–protein 10 (IP-10), platelet-derived growth factor (PDGF)-AA, PDGF-AB/BB, CCL5 (RANTES), transforming growth factor (TGF)-α, and tumor

Table 1. Real-Time PCR Primer Sequences for Human Genes

Gene Name	Forward Sequence	Reverse Sequence
HPRT1	CCTGGCGTCGTGATTAGTGAT	AGACGTTCAGTCCTGTCCATAA
MITF	AGCCATGCAGTCCGAAT	ACTGCTGCTCTTCAGCG
RLBP1	CCAGGACAGTTGAGGAGAGG	CACGCTGCCCAAGTATGATG
VEGFA	GGGCAGAATCATCACGAAGTG	ATTGGATGGCAGTAGCTGCG
SERPINF1 (*PEDF*)	TATCACCTTAACCAGCCTTTCATC	GGGTCCAGAATCTTGCAATG
SOD2	CGTTCAGGTTGTTCACGTAGG	CCTCACATCAACGCGCAGAT
OCLN	CCCTTTTAGGAGGTAGTGTAGGC	CCGTAGCCATAGCCATAACCA
ATP1A2	ACAGCCTTCTTCGTCAGTATCGT	CGAATTCCTCCTGGTCTTACAGA
MYO7A	CATGACGGGGAGTCCACAG	TCTCTTGCTAGGTTGACAGAGG
OTX2	TAAGCAACCGCCTTACG	GCACTTAGCTCTTCGATT
EZR	GTTTTCCCCAGTTGTAATAGTGCC	TCCGTAATTCAATCAGTCCTGC
BEST1	GAATTTGCAGGTGTCCCTGT	ATCCTCCTCGTCCTCCTGAT
TFEB	CGCATCAAGGAGTTGGGAAT	CTCCAGGCGGCGAGAGT
TJP-1 (*ZO-1*)	CAACATACAGTGACGCTTCACA	GACGTTTCCCCACTCTGAAAA
FGF2	ATCAAAGGAGTGTGTGCTAACC	ACTGCCCAGTTCGTTTCAGTG

Primers for *GAPDH*, *RPE65*, *THBS1*, and *NGF* were obtained from Qiagen (cat. no. PPH00150A, PPH07121A, QT00001456, PPH00205A).

necrosis factor (TNF)-α. All conditioned media samples were run in technical duplicate.

Phagocytosis

Bovine eyes were obtained from Research 87 (Boylston, MA) within 6 hours of enucleation. Photoreceptor outer segments (POS) were then isolated based on a method previously reported.[37] Thirty million POS (100 per RPE cell) were loaded into the apical media of cells cultured for 4 weeks. After 16 hours of co-incubation, samples were washed extensively with PBS to remove POS not bound to RPE. Cells were then fixed with 4% paraformaldehyde, permeabilized with 0.1% Triton X-100, and immunostained with 2 μg/mL mouse anti-rhodopsin primary antibody (EMD Millipore) overnight at 4°C. The next day cells were incubated with 10 μL/mL DAPI and 2 μg/mL AlexaFluor 594 rabbit anti-goat secondary antibody for 1 hour, washed, mounted onto glass slides, and imaged using an Axioskop MOT 2. The relative number of POS bound/internalized per cell was quantified by dividing the number of red fluorescent pixels above a threshold by the number of DAPI-stained nuclei in that area. The size of bound and phagocytosed POS in these images was also assessed using the "threshold" and "analyze particle" functions in ImageJ (National Institutes of Health, Bethesda, MD).

Statistical Analysis

All values are expressed as the mean ± standard deviation unless otherwise noted with statistical significance determined using an unpaired two-tailed Student's *t*-test. Error bars on graphs represent standard error of the mean. TER measurements were taken for 18, 10, and 2 biological replicates per condition for 1, 4, and 8 weeks, respectively. ELISAs for VEGF and PEDF were performed on cultured media collected from six experimental replicates while multiplex analysis used five replicates. All other cell culture experiments were completed in biological triplicate.

A

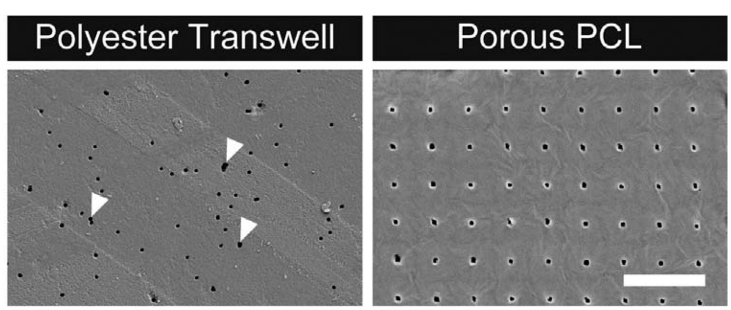

B

Porous scaffold characterization

	Polyester Transwell	Porous PCL
Pore Size (nm)	449 ± 8	532 ± 7*
Porosity (%)	0.64 ± 0.06	0.90 ± 0.05†

Figure 1. **(A)** Surface morphology of track-etched polyester transwells with randomly distributed pores and pore-cast PCL with larger regularly spaced pores imaged using SEM. *Arrows* indicate locations of fused circular pores resulting from the track etching process. *Scale bar*: 10 μm. **(B)** Table of pore size and total porosity for polyester transwells and porous PCL. $^*P < 0.05$; $†P < 0.001$.

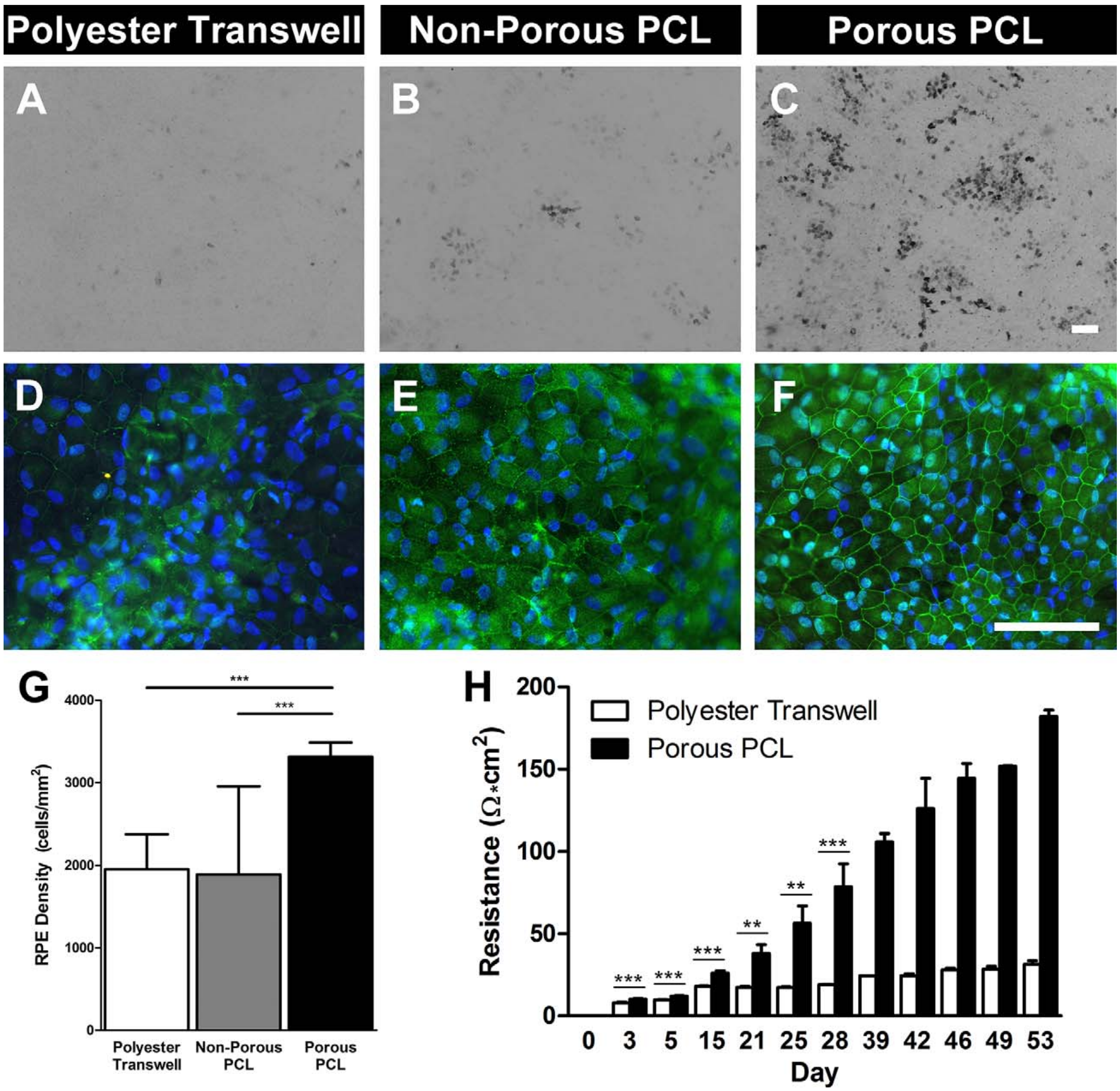

FIGURE 2. fhRPE cultured on porous PCL display improved markers of maturity including pigmentation, improved tight junction localization, increased cellular density, and superior barrier formation. Light microscopy images of (**A**) porous polyester transwell, (**B**) nonporous PCL, and (**C**) porous PCL displaying varying levels of fhRPE pigmentation at 8 weeks. Immunohistochemical staining for tight junction associated protein-1 (ZO-1, *green*) and nuclei (DAPI, *blue*) in cells cultured for 8 weeks on (**D**) porous polyester transwells, (**E**) nonporous PCL, and (**F**) porous PCL. *Scale bars*: 100 μm. (**G**) Graph indicating significantly increased RPE cellular density on porous PCL compared to either control substrate after 8 weeks. (**H**) Increased transepithelial resistance of fhRPE on porous PCL throughout the first 8 weeks of culture indicating improved barrier formation. Please note that data from >28 days is derived from only two biological replicates, so no statistical measures were used. $^{**}P < 0.01$; $^{***}P < 0.001$.

RESULTS

Scaffold Characterization

SEM was used to quantify the average pore diameter and total porosity of the substrates used in this study. Track-etched polyester transwells, the current standard RPE culture substrate in the field, contained pores close to the manufacturer's quoted size of 400 nm distributed across the surface of the membrane. Although many of these pores were circular, there was also a subset of irregular pores that appeared to have been formed by multiple overlapping circular pores (Fig. 1A, arrows), which is known to occur with a certain probability due to the track etching process.[38] Porous PCL scaffolds contained significantly larger pores ($P < 0.05$), which were spaced evenly in a grid and covered a larger percentage of the surface ($P < 0.001$). Pore size and total porosity of the porous PCL were higher than the polyester transwell control, but on the same order of magnitude (Fig. 1B). Aside from the pores, the surfaces of all three substrates were smooth and unremarkable.

Cell Appearance and Morphology

Bright field microscopy revealed little-to-no fhRPE pigmentation after 1 and 4 weeks of culture. However, after 8 weeks fhRPE cells displayed varying degrees of pigmentation depend-

Table 2. Relative Gene Expression by fhRPE After 4 Weeks of Culture

Gene Name	Polyester Transwell	Nonporous PCL	Porous PCL
MITF	1.01 ± 0.07	0.94 ± 0.07	0.85 ± 0.05
OCLN	1.00 ± 0.03	1.19 ± 0.02*	1.09 ± 0.01
ATP1A2	1.00 ± 0.03	0.74 ± 0.01†	0.91 ± 0.00
MYO7A	1.02 ± 0.15	1.14 ± 0.14	1.14 ± 0.23
OTX2	1.00 ± 0.07	1.09 ± 0.14	0.93 ± 0.06
THBS1	1.01 ± 0.14	1.55 ± 0.51	1.25 ± 0.18
TFEB	1.02 ± 0.13	0.66 ± 0.09	0.75 ± 0.04
TJP-1 (ZO-1)	1.00 ± 0.00	0.99 ± 0.09	0.94 ± 0.08
FGF2	1.00 ± 0.06	1.01 ± 0.01	1.03 ± 0.03
NGF	1.02 ± 0.14	0.80 ± 0.15	0.70 ± 0.08

* $P < 0.05$ compared to polyester transwells.
† $P < 0.01$ compared to polyester transwells.

ing on their culture substrate. Cells on porous polyester transwells displayed the least amount of pigmentation with few dark cells (Fig. 2A). A slightly higher proportion of fhRPE on nonporous PCL appeared pigmented (Fig. 2B), while the most pigmentation was observed on porous PCL (Fig. 2C). In all conditions pigmented fhRPE appeared to be localized in foci interspersed amongst nonpigmented cells. fhRPE shape and size were determined using immunostaining. ZO-1 and DAPI staining indicated that cells on all substrates generally assumed the hexagonal morphology that is characteristic of RPE, with nuclei located toward their lateral edge (Figs. 2D–F). Cell density was similar on polyester transwells and nonporous PCL, but significantly higher ($P < 0.001$) on porous PCL (Fig. 2G).

Epithelial Barrier Formation

Epithelial barrier formation was assessed using tight junction staining (ZO-1) and TER measurements. ZO-1 staining of fhRPE cultured for 8 weeks on polyester transwells was generally diffuse, though faint localization was observed at cell borders (Fig. 2D). Cells on nonporous PCL displayed moderate ZO-1 localization at cell–cell borders but again showed a considerable amount of diffuse staining (Fig. 2E). In comparison, ZO-1 staining of fhRPE on porous PCL was more intense and continuous at the cell–cell border indicating the formation of mature tight junctions (Fig. 2F). This improvement in tight junction formation was quantitatively confirmed by TER measurement. Figure 2H illustrates the progression of cell-derived electrical resistance over the course of 8 weeks. At all time points other than day 0, fhRPE on porous PCL exhibited a significantly higher resistance than cells on polyester transwells ($P < 0.01$); however, the statistics for time points greater than 28 days were not counted due to the limited number of biological duplicates used ($n = 2$). The resistance of fhRPE on transwells increased slowly, whereas the resistance of cells on porous PCL increased rapidly and continued to increase through 8 weeks of culture at which point RPE cultured on polyester and porous PCL achieved TER values of 31 ± 2 and 182 ± 4 $\Omega \cdot cm^2$, respectively.

Gene Expression

mRNA analysis of fhRPE cultured for 4 weeks on each substrate revealed several differentially expressed genes associated with RPE differentiation, homeostasis, and function. While a majority of the genes tested did not display major differences between culture substrates (Table 2), many genes critically involved in RPE visual or neurotrophic functions such as *RPE65*, *RLBP1*, *BEST1*, and *SERPINF1* (*PEDF*) were strongly up-regulated in cells cultured on porous PCL compared to polyester transwells (Fig. 3). The antioxidant enzyme SOD2 was also down-regulated approximately 50% on porous PCL compared with polyester transwells (Fig. 3A).

Protein Secretion

Secretion of the major fhRPE-produced growth factors, VEGF and PEDF, was characterized over time by ELISA. As expected, a significant increase in the secretion of both cytokines was observed during RPE maturation in all conditions (Figs. 4A, 4B). In addition, both VEGF and PEDF secretion were highest on porous PCL, mimicking the results obtained at the mRNA level (Fig. 3) and suggesting that the production of these growth factors are largely controlled at the transcriptional level. The cell culture substrate used also affected the polarization of growth factor secretion. fhRPE cultured on polyester transwells obtained higher apical media concentrations of VEGF and higher basal media concentrations of PEDF relative to the adjacent chamber (Table 3). Alternately, cells on porous PCL assumed a secretion profile more characteristic of in vivo RPE, with higher levels of VEGF in the basal media and higher levels of PEDF in the apical media.[39,40]

A multiplex ELISA was used to determine the production of inflammatory cytokines by fhRPE on each substrate in order to better evaluate the clinical potential of porous PCL scaffolds for RPE transplantation. Most of the cytokines analyzed were not detected in conditioned media, indicating minimal production (Table 4). The analytes that were present above the minimum threshold for detection were EGF, CX3CL1, CXCL1, IL-6, and PDGF-AA, all of which were produced in similar amounts by fhRPE on polyester transwells and porous PCL.

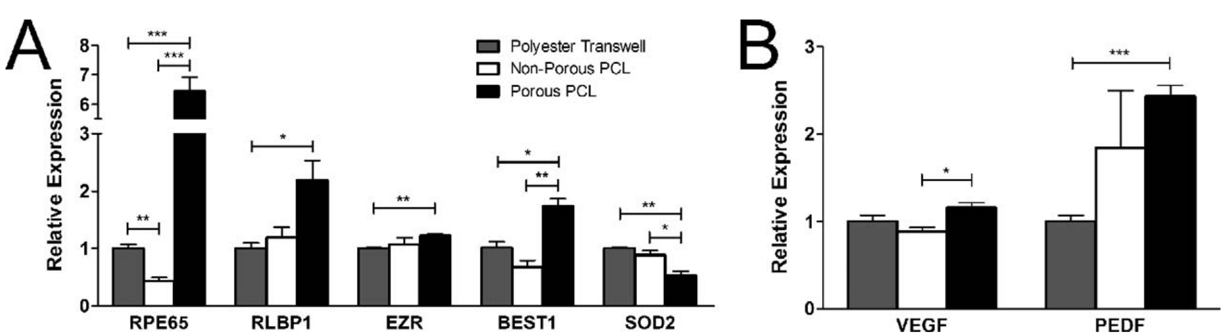

Figure 3. Relative expression of genes associated with RPE (A) function and (B) growth factor production are up-regulated in fhRPE cultured on porous PCL for 4 weeks. *$P < 0.05$; **$P < 0.01$; ***$P < 0.001$.

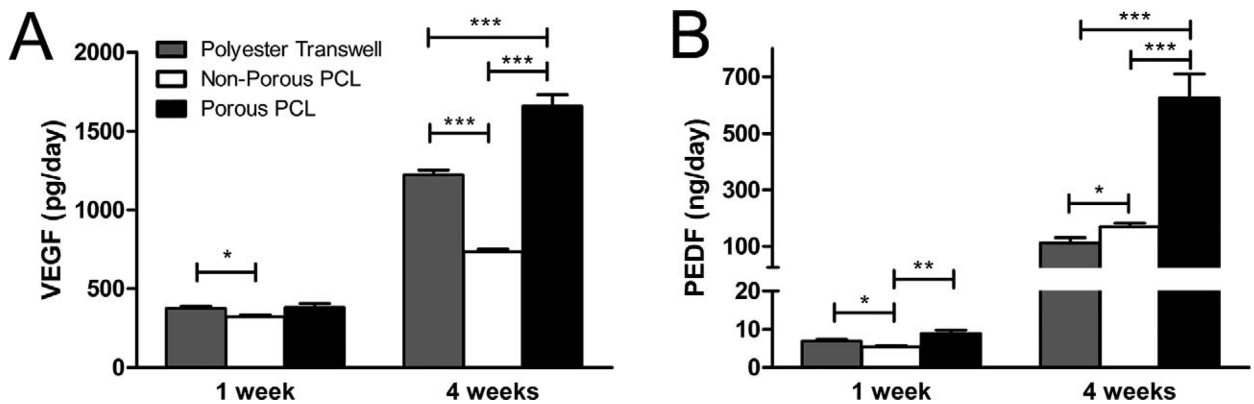

FIGURE 4. VEGF and PEDF secretion by fhRPE is dependent on both culture duration and substrate. (A) VEGF and (B) PEDF secretion are highest on porous PCL at 4 weeks. $^{*}P < 0.05$; $^{**}P < 0.01$; $^{***}P < 0.001$.

Phagocytosis

Finally, we evaluated the effect of culture substrate on RPE phagocytic function by quantifying the number and size of bovine POS bound to or internalized by fhRPE at steady-state (Fig. 5). Phagocytosis expressed as rhodopsin-labeled fluorescence per cell (analogous to POS bound/internalized per cell) revealed no statistically significant difference between fhRPE cultured for 4 weeks on any of the substrates (Fig. 5D). However, POS fragments were significantly smaller and more numerous on porous PCL compared to polyester transwells ($P < 0.01$, Fig. 5E). For all conditions the average POS size on each substrate was within the range of individual rod (0.8–4.9 μm^2) and cone (1.1–9.6 μm^2) POS.[41,42]

DISCUSSION

This study demonstrates that porous PCL scaffolds enhance fhRPE morphology, cell density, barrier formation, gene expression, and protein secretion compared to cells on nonporous PCL or porous polyester. Pigmentation has been widely used as an overt marker of RPE maturity[43] and also serves a functional role by absorbing light to minimize scatter for improved vision.[44] Therefore, increased pigmentation observed in fhRPE on porous PCL serves as an indication that these cells are more mature and functional, at least in terms of light absorption.

Immunohistochemistry revealed that fhRPE achieved a monolayer of cells with characteristic hexagonal morphology on all three substrates; however, tight junction staining was most intense at the cell–cell junction on porous PCL. Intense ZO-1 staining, like that seen on porous PCL, has been associated with the native macular RPE, while low-intensity staining, like that observed on porous polyester transwells, is characteristic of peripheral RPE.[45] fhRPE on porous PCL achieved an average cell density of 3317 ± 171 cells/mm^2, which was between the average cell density previously reported for the midperiphery (3002 ± 460 cell/mm^2) and fovea (4220–4980 cells/mm^2).[46,47] Comparatively, fhRPE on porous polyester transwells and nonporous PCL were less densely packed than on porous PCL and similar to the cell density found at the periphery (1600 ± 411 cells/mm^2).[46] As a result, RPE cultured on porous PCL are likely more suitable for submacular RPE replacement therapies that require densely packed, high-functioning cells similar to native central RPE.

fhRPE on porous PCL also displayed more complete and uniform tight junction staining indicating the formation of a well-developed barrier. This qualitative observation was reinforced by TER measurements, which demonstrated that RPE on porous PCL provided more resistance than cells on porous polyester transwells at every time point beyond day 0. Because barrier formation is required for many homeostatic functions including fluid transport, maintenance of the blood–retinal barrier, and polarized growth factor secretion,[44] this improvement on porous PCL may be especially critical for success in RPE-based transplantation therapies.

Gene expression analysis provided further indications of improved RPE maturity and function on porous PCL. Many genes associated with RPE differentiation, maturation, or function such as *EZR*, *BEST1*, *RPE65*, and *RLBP1* were significantly up-regulated in cells cultured on porous PCL. Interestingly the enzyme SOD2, which acts as an antioxidant in the RPE,[48] was down-regulated on porous PCL suggesting that these cells may be under less oxidative stress than cells on either control material. Both VEGF and PEDF secretion levels were similar to what has been previously reported for fhRPE.[49] While changes in VEGF expression were rather minor and unlikely to result in major physiological differences, PEDF expression was highly up-regulated on porous PCL compared to polyester transwells. Because PEDF serves two functions as both a neurotrophic and anti-angiogenic factor,[3,50] up-regulation on porous PCL may indicate a superior ability to both support photoreceptors and maintain neuroretinal avascularity in cell-based AMD therapies.

The production of inflammatory cytokines by fhRPE on all substrates was very low compared to VEGF and PEDF. The inflammatory cytokines CX3CL1, CXCL1, and IL-6 were all

TABLE 3. VEGF and PEDF Concentrations (ng/mL) Produced in 72 Hours by fhRPE After 4 Weeks of Culture

	Apical VEGF	Basal VEGF	Apical PEDF	Basal PEDF
Porous polyester	2.14 ± 0.14	1.73 ± 0.14	122 ± 66	183 ± 87
Nonporous PCL	4.40 ± 0.24*	0†	1010 ± 192	0†
Porous PCL	2.34 ± 0.32	2.54 ± 0.34*	996 ± 317*	918 ± 322*

* $P < 0.001$ compared to polyester transwells.
† Zero value due to nonporous substrate.

Table 4. Total Inflammatory Cytokine Production (pg/d) by fhRPE After 4 Weeks of Culture

	Porous Transwell	Nonporous PCL	Porous PCL
EGF	2.07 ± 0.29	0.77 ± 0.29*	2.08 ± 0.55
Eotaxin	ND	ND	ND
FGF-2	ND	ND	ND
CX3CL1, fractalkine	29.19 ± 4.77	20.92 ± 2.40	34.36 ± 2.89
G-CSF	ND	ND	ND
GM-CSF	ND	ND	ND
CXCL1, GRO	31.26 ± 2.63	28.88 ± 1.42	26.93 ± 3.46
IL-1α	ND	ND	ND
IL-1β	ND	ND	ND
IL-1RA	ND	ND	ND
IL-6	15.21 ± 1.78	13.38 ± 0.74	12.08 ± 0.97
IL-8	ND	ND	ND
IL-15	ND	ND	ND
IP-10	ND	ND	ND
PDGF-AA	262.30 ± 9.92	245.50 ± 7.93	243.30 ± 13.47
PDGF-AB/BB	ND	ND	ND
CCL5, RANTES	ND	ND	ND
TGF-α	ND	ND	ND
TNF-α	ND	ND	ND

ND, not detected (<2.2 pg/d).
*$P < 0.001$ compared to polyester transwells.

produced in such minimal amounts relative to serum levels that they would be negligible in vivo.[51–53] fhRPE on all three substrates secreted PDGF-AA at a similar rate which was approximately 5-fold higher than what has been reported for quiescent fhRPE, but much lower than the level produced by fhRPE after TGF-β stimulation.[54] In general, this analysis suggests that culture on porous PCL is unlikely to significantly affect intrinsic inflammatory cytokine secretion by RPE.

Although the total steady-state fluorescence from bound and internalized POS was similar on all substrates, fluorescent fragment size was significantly decreased on porous PCL compared to polyester transwells. After POS discs are shed by photoreceptors and internalized by RPE they enter the phagolysosome where they are degraded into their component proteins, peptides, and lipids. Therefore, the presence of smaller, more numerous fluorescent fragments in fhRPE suggests that POS on porous PCL are further along in the process of degradation due to more rapid processing. This type of improvement in POS degradation on porous PCL would be especially beneficial from a translational perspective because inadequate processing has been cited as a possible cause of material accumulation in BrM eventually resulting in RPE atrophy.[14]

Overall, the results of this study indicate that porous PCL enhances fhRPE maturation compared to both nonporous PCL and polyester transwells. Improvements in RPE phenotype and function were observed for all analysis methods used except phagocytosis, which displayed minor, but statistically insignificant improvements on porous PCL. Interestingly, it appears that both substrate composition and porosity have an effect on fhRPE behavior. fhRPE on porous PCL exhibited improved markers of maturation and function compared with cells on porous polyester, suggesting that PCL is a superior RPE substrate for in vitro culture. However, RPE on nonporous PCL did not experience the same improvements as cells on porous PCL, suggesting that substrate porosity also has a beneficial effect on behavior. BrM porosity and permeability decrease with age or disease, suggesting that impaired basal RPE flux may play a role in RPE dysfunction.[55,56] Although reduced flux in vivo is likely due to BrM thickening, cross-linking, or high lipid content, nonporous artificial RPE substrates are likely to have the same effect in vitro, leading to reduced cell function. Instead, substrates that more closely approximate the porosity of healthy native BrM, such as porous

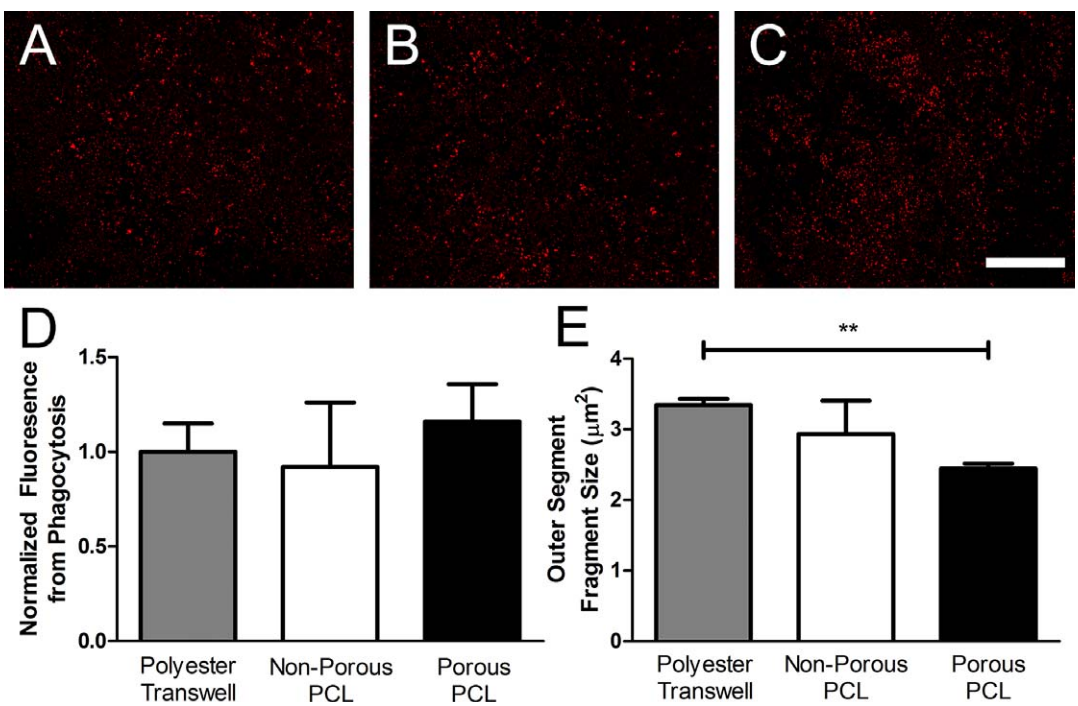

Figure 5. Culture substrate did not affect the POS phagocytosis or binding capacity of fhRPE but altered POS fragment size. Micrographs of rhodopsin-stained POS bound or internalized by fhRPE cultured for 4 weeks on (**A**) polyester transwells, (**B**) nonporous PCL, and (**C**) porous PCL. (**D**) Quantification of POS uptake and (**E**) fragment size using rhodopsin antibody-based fluorescence. *Scale bar*: 500 μm. **$P < 0.01$.

PCL, are likely to achieve appropriate basal RPE flux and elicit improved cell behavior or function.

As a result, porous PCL, which benefits from both material composition and porosity, is an attractive scaffold for RPE maturation and delivery in cell-based dry AMD therapies. In addition to its subretinal biocompatibility[26,31] and appropriate mechanical properties for surgical handling, we have now shown that porous PCL also improves RPE cell maturation, which may be critical in reestablishing normal tissue function. Future studies will aim to deliver an established monolayer of RPE on porous PCL into the subretinal space of animals with nonfunctional or atrophic RPE to determine the in vivo function of transplanted RPE.

Acknowledgments

The authors thank Jinmei Wang for POS isolation.

Supported by the National Institutes of Health (NIH) through the NIH Director's New Innovator Award Program, 1-DP2-OD006649 (MSG), and award number 5-T32-EB006359-05 from the National Institute of Biomedical Imaging and Bioengineering (KM). The content is solely the responsibility of the authors and does not necessarily represent the official views of the National Institutes of Health or National Institute of Biomedical Imaging and Bioengineering.

Disclosure: **K.J. McHugh**, The Charles Stark Draper Laboratory, Inc. (E); **S.L. Tao**, The Charles Stark Draper Laboratory, Inc. (E), CooperVision, Inc. (E), P; **M. Saint-Geniez**, P

References

1. Jager RD, Mieler WF, Miller JW. Age-related macular degeneration. *N Engl J Med*. 2008;358:2606–2617.
2. Nowak JZ. Age-related macular degeneration (AMD): pathogenesis and therapy. *Pharmacol Rep*. 2006;58:353–363.
3. Strauss O. The retinal pigment epithelium in visual function. *Physiol Rev*. 2005;85:845–881.
4. Binder S, Stanzel BV, Krebs I, Glittenberg C. Transplantation of the RPE in AMD. *Prog Retin Eye Res*. 2007;26:516–554.
5. Shiragami C, Matsuo T, Shiraga F, Matsuo N. Transplanted and repopulated retinal pigment epithelial cells on damaged Bruch's membrane in rabbits. *Br J Ophthalmol*. 1998;82:1056–1062.
6. Ramrattan RS, van der Schaft TL, Mooy CM, de Bruijn WC, Bulder PG, de Jong PT. Morphometric analysis of Bruch's membrane, the choriocapillaris, and the choroid in aging. *Invest Ophthalmol Vis Sci*. 1994;35:2857–2864.
7. Moore DJ, Hussain AA, Marshall J. Age-related variation in the hydraulic conductivity of Bruch's membrane. *Invest Ophthalmol Vis Sci*. 1995;36:1290–1297.
8. Curcio CA, Johnson M. Structure, function, and pathology of Bruch's membrane. In: Ryan SJ, ed. *Retina: Expert Consult Premium Edition*. Oxford: Elsevier;2013;465–481.
9. Pauleikhoff D, Harper CA, Marshall J, Bird AC. Aging changes in Bruch's' membrane. A histochemical and morphologic study. *Ophthalmology*. 1990;97:171–178.
10. Marshall GE, Konstas AG, Reid GG, Edwards JG, Lee WR. Type IV collagen and laminin in Bruch's membrane and basal linear deposit in the human macula. *Br J Ophthalmol*. 1992;76:607–617.
11. Tezel TH, Kaplan HJ, Del Priore LV. Fate of human retinal pigment epithelial cells seeded onto layers of human Bruch's membrane. *Invest Ophthalmol Vis Sci*. 1999;40:467–476.
12. Tezel TH, Del Priore LV. Repopulation of different layers of host human Bruch's membrane by retinal pigment epithelial cell grafts. *Invest Ophthalmol Vis Sci*. 1999;40:767–774.
13. Cai H, Del Priore LV. Bruch membrane aging alters the gene expression profile of human retinal pigment epithelium. *Curr Eye Res*. 2006;31:181–189.
14. Sun K, Cai H, Tezel TH, Paik D, Gaillard ER, Del Priore LV. Bruch's membrane aging decreases phagocytosis of outer segments by retinal pigment epithelium. *Mol Vis*. 2007;13:2310–2319.
15. Gullapalli VK, Sugino IK, Van Patten Y, Shah S, Zarbin MA. Impaired RPE survival on aged submacular human Bruch's membrane. *Exp Eye Res*. 2005;80:235–248.
16. Hynes SR, Lavik EB. A tissue-engineered approach towards retinal repair: scaffolds for cell transplantation into the subretinal space. *Graefes Arch Clin Exp Ophthalmol*. 2010;248:763–778.
17. Del Priore LV, Tezel TH, Kaplan HJ. Survival of allogeneic porcine retinal pigment epithelial sheets after subretinal transplantation. *Invest Ophthalmol Vis Sci*. 2004;45:985–992.
18. Giordano GG, Thomson RC, Ishaug SL, et al. Retinal pigment epithelium cells cultured on synthetic biodegradable polymers. *J Biomed Mater Res*. 1997;34:87–93.
19. Singh S, Woerly S, McLaughlin BJ. Natural and artificial substrates for retinal pigment epithelial monolayer transplantation. *Biomaterials*. 2001;22:3337–3343.
20. Lutolf MP, Hubbell JA. Synthetic biomaterials as instructive extracellular microenvironments for morphogenesis in tissue engineering. *Nat Biotechnol*. 2005;23:47–55.
21. Lu L, Mikos AG. The importance of new processing techniques in tissue engineering. *MRS Bull*. 1996;21:28–32.
22. Saint-Geniez M, Tao SL, Tucker BT, et al. Retina reconstruction. In: Ducheyne P, Healy K, Hutmacher DE, Grainger DW, Kirkpatrick CJ, eds. *Comprehensive Biomaterials*. Waltham, MA: Elsevier; 2011;500–516.
23. Liu X, Holzwarth JM, Ma PX. Functionalized synthetic biodegradable polymer scaffolds for tissue engineering. *Macromol Biosci*. 2012;12:911–919.
24. Thomson HA, Treharne AJ, Walker P, Grossel MC, Lotery AJ. Optimisation of polymer scaffolds for retinal pigment epithelium (RPE) cell transplantation. *Br J Ophthalmol*. 2011;95:563–568.
25. Gunatillake PA, Adhikari R. Biodegradable synthetic polymers for tissue engineering. *Eur Cell Mater*. 2003;5:1–16.
26. Christiansen AT, Tao SL, Smith M, et al. Subretinal implantation of electrospun, short nanowire, and smooth poly(ε-caprolactone) scaffolds to the subretinal space of porcine eyes. *Stem Cells Int*. 2012;2012:454295.
27. Sabir MI, Xu X, Li L. A review on biodegradable polymeric materials for bone tissue engineering applications. *J Mater Sci*. 2009;44:5713–5724.
28. Kohn J, Abramson S, Langer R. Bioresorbable and bioerodible materials. In: Ratner BD, Hoffman AS, Schoen FJ, Lemons JE, eds. *Biomaterials Science: An Introduction to Materials in Medicine*. 2nd ed. Boston, MA: Elsevier Academic Press; 2004;115–126.
29. Tao S, Young C, Redenti S, et al. Survival, migration and differentiation of retinal progenitor cells transplanted micromachined poly(methyl methacrylate) scaffolds to the subretinal space. *Lab Chip*. 2007;7:695–701.
30. Montezuma SR, Loewenstein J, Scholz C, Rizzo JF 3rd. Biocompatibility of materials implanted into the subretinal space of Yucatan pigs. *Invest Ophthalmol Vis Sci*. 2006;47:3514–3522.
31. Redenti S, Tao S, Yang J, et al. Retinal tissue engineering using mouse retinal progenitor cells and a novel biodegradable, thin-film poly(e-caprolactone) nanowire scaffold. *J Ocul Bio Dis Infor*. 2008;1:19–29.
32. Redenti S, Neeley WL, Rompani S, et al. Engineering retinal progenitor cell and scrollable poly(glycerol-sebacate) compos-

ites for expansion and subretinal transplantation. *Biomaterials*. 2009;30:3405–3414.

33. Pachence JM, Bohrer MP, Kohn J. Biodegradable polymers. In: Lanza R, Langer R, Vacanti J, eds. *Principles of Tissue Engineering*. 3rd ed. Burlington, MA: Elsevier Academic Press; 2007;323–340.
34. Salgado CL, Sanchez EM, Zavaglia CA, Granja PL. Biocompatibility and biodegradation of polycaprolactone-sebacic acid blended gels. *J Biomed Mater Res A*. 2012;100:243–251.
35. McHugh KJ, Tao SL, Saint-Geniez M. Topographical control of ocular cell types for tissue engineering. *J Biomed Mater Res B*. 2013;doi: 10.1002/jbm.b.32968.
36. McHugh KJ, Tao SL, Saint-Geniez M. A novel porous scaffold fabrication technique for epithelial and endothelial tissue engineering. *J Mater Sci Mater Med*. 2013;24:1659–1670.
37. Tsang SH, Burns ME, Calvert PD, et al. Role for the target enzyme in deactivation of photoreceptor G protein in vivo. *Science*. 1998;282:117–121.
38. Quinn JA, Anderson JL, Ho WS, Petzny WJ. Model pores of molecular dimension: the preparation and characterization of track-etched membranes. *Biophys J*. 1972;12:990–1007.
39. Blaauwgeers HG, Holtkamp GM, Rutten H, et al. Polarized vascular endothelial growth factor secretion by human retinal pigment epithelium and localization of vascular endothelial growth factor receptors on the inner choriocapillaris. Evidence for a trophic paracrine relation. *Am J Pathol*. 1999;155: 421–428.
40. Maminishkis A, Chen S, Jalickee S, et al. Confluent monolayers of cultured human fetal retinal pigment epithelium exhibit morphology and physiology of native tissue. *Invest Ophthalmol Vis Sci*. 2006;47:3612–3624.
41. Polyak SL. *The Retina*. Chicago: University of Chicago Press; 1941.
42. Young RW. The renewal of rod and cone outer segments in the rhesus monkey. *J Cell Biol*. 1971;49:303–318.
43. Vaajasaari H, Ilmarinen T, Juuti-Uusitalo K, et al. Toward the defined and xeno-free differentiation of functional human pluripotent stem cell-derived retinal pigment epithelial cells. *Mol Vis*. 2011;17:558–575.
44. Marmor MF. Retinal pigment epithelium. Yanoff M, Duker JS, eds. *Ophthalmology: Expert Consult Premium Edition*. 3rd ed. Oxford: Mosby Elsevier; 2008:515–517.
45. Kokkinopoulos I, Shahabi G, Colman A, Jeffery G. Mature peripheral RPE cells have an intrinsic capacity to proliferate; a potential regulatory mechanism for age-related cell loss. *PLoS One*. 2011;6:e18921.
46. Panda-Jonas S, Jonas JB, Jakobczyk-Zmija M. Retinal pigment epithelial cell count, distribution, and correlations in normal human eyes. *Am J Ophthalmol*. 1996;121:181–189.
47. Del Priore LV, Kuo YH, Tezel TH. Age-related changes in human RPE cell density and apoptosis proportion in situ. *Invest Ophthalmol Vis Sci*. 2002;43:3312–3318.
48. Newsome DA, Dobard EP, Liles MR, Oliver PD. Human retinal pigment epithelium contains two distinct species of superoxide dismutase. *Invest Ophthalmol Vis Sci*. 1990;31:2508–2513.
49. Ablonczy Z, Dahrouj M, Tang PH, et al. Human retinal pigment epithelium cells as functional models for the RPE in vivo. *Invest Ophthalmol Vis Sci*. 2011;52:8614–8620.
50. McKay BS, Goodman B, Falk T, Sherman SJ. Retinal pigment epithelial cell transplantation could provide trophic support in Parkinson's disease: results from an in vitro model system. *Exp Neurol*. 2006;201:234–243.
51. Suzuki F, Kubota T, Miyazaki Y, et al. Serum level of soluble CX3CL1/fractalkine is elevated in patients with polymyositis and dermatomyositis, which is correlated with disease activity. *Arthritis Res Ther*. 2012;14:R48.
52. Takahashi K, Ohara M, Sasai T, et al. Serum CXCL1 concentrations are elevated in type 1 diabetes mellitus, possibly reflecting activity of anti-islet autoimmune activity. *Diabetes Metab Res Rev*. 2011;27:830–833.
53. Cao S, Walker GB, Wang X, Cui JZ, Matsubara JA. Altered cytokine profiles of human retinal pigment epithelium: oxidant injury and replicative senescence. *Mol Vis*. 2013;19: 718–728.
54. Nagineni CN, Kutty V, Detrick B, Hooks JJ. Expression of PDGF and their receptors in human retinal pigment epithelial cells and fibroblasts: regulation by TGF-beta. *J Cell Physiol*. 2005; 203:35–43.
55. Moore DJ, Clover GM. The effect of age on the macromolecular permeability of human Bruch's membrane. *Invest Ophthalmol Vis Sci*. 2001;42:2970–2975.
56. Zayas-Santiago A, Marmorstein AD, Marmorstein LY. Relationship of Stokes radius to the rate of diffusion across Bruch's membrane. *Invest Ophthalmol Vis Sci*. 2011;52:4907–4913.